Gray/Nongray Gas Radiation Modeling in Steam Cracker CFD Calculations

G. D. Stefanidis
Laboratorium voor Petrochemische Techniek (LPT), Ghent University, Krijgslaan 281 Block S5, Ghent B9000, Belgium

B. Merci
Vakgroep Mechanica van Stroming, Warmte en Verbranding, Ghent University, St. Pietersnieuwstraat 41, Ghent B9000, Belgium

G. J. Heynderickx and G. B. Marin
Laboratorium voor Petrochemische Techniek (LPT), Ghent University, Krijgslaan 281 Block S5, Ghent B9000, Belgium

DOI 10.1002/aic.11186
Published online May 9, 2007 in Wiley InterScience (www.interscience.wiley.com).

A constant composition gray gas and a constant composition nongray gas radiation model are developed and applied in computational fluid dynamic simulations of an industrial scale steam cracking furnace. Both models are based on the exponential wide band model. The gray gas model simplification, commonly used for simulations of industrial applications, is found to have an effect on predicted variable fields like flue gas flow, temperature, and heat flux to the reactor tubes. When the nongray gas model is used, higher energy absorption by the flue gas in the furnace and lower energy transfer to the process gas in the reactor tubes is calculated because of the high absorption coefficients in the strongly absorbing bands of 2.7 and 4.3 μm. Thus, the calculated thermal efficiency increases from 37.5% when using the nongray gas model to 42.6% when using the gray gas model. A 5% difference in the thermal efficiency is large considering the scale and the importance of the process and should be taken into account by the furnace designer. It is also shown that although both models reproduce the basic characteristics of the flow pattern in the furnace, quantitative differences in the flue gas speed are predicted in some regions of the furnace domain. © 2007 American Institute of Chemical Engineers *AIChE J,* 53: 1658–1669, 2007

Keywords: steam cracking furnaces, heat transfer, radiation, nongray gas model, CFD

Introduction

Production of olefins by steam cracking of hydrocarbons is one of the most important processes in the petrochemical industry. The feedstock can range anywhere from light distillate fractions such as ethane or propane via naphtha or gas oil up to vacuum gas oil and gas condensates. Steam cracking is an endothermic process carried out in tubular reactor coils suspended in the radiation section of large gas-fired furnaces. Typical length, width, and height of such furnaces are approximately 12, 3, and 8 m. The heat that is required for the process is supplied by means of gaseous fuel combustion in flame burners in the furnace floor and/or in furnace side wall radiation burners.

Correspondence concerning this article should be addressed to G. J. Heynderickx at geraldine.heynderickx@UGent.be.
Current address of G. D. Stefanidis: Dept. of Chemical Engineering and Center for Catalytic Science and Technology (CCST), University of Delaware, Newark, DE 19716

In the Laboratorium voor Petrochemische Techniek (LPT) a complete software package has been developed over the last 20 years for simulation of all processes taking place in a steam cracking furnace. This ongoing research has resulted in several publications in the open literature concerning "process-side" modeling,[1] "fire-side" modeling,[2] as well as complete furnace simulations.[3,4]

In this work, the focus is on improving the modeling of radiative heat transfer in the context of computational fluid dynamic (CFD) calculations on the flue gas side of a steam cracking furnace. Accurate calculation of the radiative heat fluxes in the furnace domain is of paramount importance, since over 90% of the total heat transfer from the furnace to the process gas in the reactor coils is because of radiation. One of the most important issues of gas radiation is the description of the radiative properties of real or so-called nongray gases. In a condensed review of the issue, three main classes of models for estimation of radiative properties of gases can be identified. They are presented here in order of decreasing complexity.

1. The spectral line-by-line (SLBL) models.
2. The spectral band (SB) models.
3. The gray gas models.

The SLBL models calculate the radiative properties for each individual absorption line,[5] and they usually rely on the HITRAN database.[6] Since a rotational and vibrational band encompasses thousands of absorption lines, this approach is far too expensive from a computational point of view for engineering applications. At present, SLBL models are used only for benchmark solutions to validate the approximate methods.

The SB models divide the whole wavelength spectrum ($\sim$0.7–25 μm, where the vibration–rotation transitions in gases occur) into a number of absorbing/emitting spectral intervals (bands) over which the radiative properties are averaged. Depending on the spectral resolution, the SB models can be classified into narrow band (NB) models and wide band (WB) models. The NB models yield very accurate solutions for high temperature gases. Although they are computationally more efficient than the SLBL method, they still require a large number of bands that render them very expensive for computation. The most popular NB models are the Elsasser model[7,8] and several statistical models.[8–10] The WB models make use of the fact that even within a wide spectral interval the black body radiation intensity can be approximated as being constant. In principle, WB correlations are derived by integrating NB results across an entire band and still provide sufficient accuracy. The exponential WB model (EWBM)[11] is the most celebrated model of this category and it will be discussed in more detail in the next paragraph. Another band based method that has gained some popularity over the last years is the κ-distribution method[12] and its extension to nonhomogeneous media the so-called correlated κ-method.[13,14] In the κ-distribution method, the spectrum is divided into a number of sufficiently NBs so that the Planck function can be considered as constant in the band. Thus, in a sufficiently NB the radiation intensity I is considered to vary only with the absorption coefficient κ. The model makes use of the idea that the absorption coefficient, which can considerably vary even within very small wavelength intervals, can be reordered in frequency so that it forms a monotonously increasing function. Then, the integration over wave number can be replaced by integration over absorption coefficient, which yields a smoother function to integrate, and can be approximated by an N-point quadrature. A complete description is given by Modest.[8]

In contrast to the band (nongray gas) models mentioned above, gray gas models provide total radiative property values, which are derived through weighted sum of spectral or band properties over the entire wavelength spectrum. Two well known models that can be implemented as gray gas models are the weighted sum of gray gases (WSGG) model[15] and the spectral line-based weighted sum of gray gases (SLW) model that was more recently developed by Denison and Webb.[16] However, WSGG can also be implemented as a SB model when solving the radiative transfer equation (RTE) for every gray gas.[17] The SLW model is a more accurate version of the WSGG model, with its parameters being calculated from a line-by-line database. As described by Modest,[8] the SLW model can also be interpreted as an implementation of the full-spectrum κ-method, and can as such be categorized with the SB models.

Gray gas modeling requires a one time solution of the RTE over the entire wavelength spectrum using an average absorption coefficient. This results in fast radiative calculations. For this reason it is by far the most widely used approach in practical combustion systems where modeling of the simultaneously occurring flow, chemical reaction and heat transfer is required. In fact, despite the well known limitations of gray gas models, there are very few papers that report on radiative heat transfer from nongray gases in three-dimensional domains.[17,18]

In the present article, constant composition gray and nongray gas calculations based on the EWBM are performed for an industrial scale steam cracking furnace segment using a commercial CFD code (FLUENT) and user defined functions. Carbon dioxide and water vapor are considered as the only components of the combustion gases that absorb and emit radiation. All details of the modeling procedure are given in the following sections. The target is to quantify the effect of the gray gas approximation on important predicted variable fields like flue gas flow, temperature, and heat flux to the reactor tubes. These are important parameters for the optimal design and operation of the furnace.

Exponential Wide-Band Model

Calculation of band transmittance

The EWBM provides a mathematical model to correlate experimental data and predict WB properties. It is based on the assumption that the rotation lines in the band are equally spaced and can be reordered in frequency so that they form an array with exponentially decreasing line intensities starting from the band center. Three parameters are required to specify the radiative properties: the integrated band intensity, $\alpha = \int_0^\infty (S/d)d(\nu_0 - \nu)$; the exponential decay width, ω; and the mean line width to spacing (a "line overlap") parameter $\beta = \pi\gamma_0/d$.

The mean line intensity to spectral line spacing ratio is given by Eq. 1 in case of an asymmetric band with the lower limit ν_l specified, by Eq. 2 in case of an asymmetric band

with the upper limit ν_u specified, or by Eq. 3 in case of a symmetric band with the band center ν_c specified.

$$S/d = (\alpha/\omega)e^{-(\nu-\nu_l)/\omega} \tag{1}$$

$$S/d = (\alpha/\omega)e^{-(\nu_u-\nu)/\omega} \tag{2}$$

$$S/d = (\alpha/\omega)e^{-2|(\nu-\nu_c)|/\omega} \tag{3}$$

Theoretically, α, β, and ω vary with temperature and pressure within each band. The EWBM however assumes variation only with respect to temperature. The pressure dependence is taken into account through the P_e number (Eq. 4).

$$P_e = \{[P/P_0][1 + (b-1)x]\}^n \tag{4}$$

Expressions for the functional dependence of α, β, and ω have been developed elsewhere[11,19] and are not cited here.

Four region expression

Originally, Edwards[11] provided correlations to a body of experimental data for the calculation of the band transmittance. The set of correlations consists of relations of linear, square root, and logarithmic form with respect to the optical depth at the band head depending on the level of absorption strength of the band. The so-called four region expression (Eqs. 5–8) is given below.

$$A^* = \tau_H \quad \text{for} \quad \tau_H \le 1 \le \eta \text{ or } \tau_H \le \eta \le 1 \quad \text{(linear regime)} \tag{5}$$

$$A^* = (4\eta\tau_H)^{1/2} - \eta \quad \text{for} \quad \eta \le \tau_H \le 1/\eta \text{ with } \eta \le 1 \quad \text{(square root regime)} \tag{6}$$

$$A^* = \ln(\tau_H\eta)^{1/2} + 2 - \eta \quad \text{for} \quad 1/\eta \le \tau_H \le \infty \text{ with } \eta \le 1 \quad \text{(logarithmic regime)} \tag{7}$$

$$A^* = \ln \tau_H + 1 \quad \text{for} \quad \tau_H \ge 1 \text{ and } \eta \le 1 \quad \text{(logarithmic regime)} \tag{8}$$

where $A^* = A/\omega$ is the dimensionless band absorption, $\tau_H = \alpha X/\omega$ is the maximum optical depth at the band head and $\eta = \beta P_e$. The band absorption or "effective" bandwidth A can be interpreted as the width of a black band (i.e. completely absorbing band) centered about the middle of the real absorption band that produces the same absorption as the real band does. The band transmittance is calculated from

$$\tau_k = \frac{\tau_H}{A^*}\frac{dA^*}{d\tau_H} \tag{9}$$

and the bandwidth from

$$\Delta\nu = A/(1-\tau_k) \tag{10}$$

Use of Eq. 9 implies a gray gas assumption for each band that breaks down at small beam lengths. For that reason, Edwards[11] suggests an upper limit for the calculation of the band transmittance (Eq. 11).

$$\tau_k = \min(\tau_k, 0.9) \tag{11}$$

Imposing an upper limit for the band transmittance may introduce serious mistakes when a recursive relationship is used due to the strong dependence on the grid resolution.[20] One way to mitigate the problem is to define the band limits from the average properties of the domain in a preprocessing step. Then the band transmittance can be calculated from Eq. 12.

$$\tau_k = 1 - A/\Delta\nu_{fix} \tag{12}$$

Using the latter approach, the band absorption A is still calculated from the four-region expression (Eqs. 5–8) and the temperature and composition dependence are still taken into account. However, instead of calculating the band transmittance from Eq. 9 in a first step, the bandwidth $\Delta\nu_{fix}$ is computed from the average properties of the domain as a first step.

Gray gas modeling

In principle, there are three approaches to calculate total radiation properties in the context of gray gas EWB modeling. These are the block calculation procedure (BCP),[11] the block approximation (BA) method,[19] and the band energy approximation (BEA) method.[21] All three methods are discussed by Nilson and Sundén.[22] The BA method is used in this work for gray gas modeling and is briefly described below. First the band absorption $A_k = A_k^* \omega_k$ of each band is determined. The total absorptance is then calculated from Eq. 13.

$$\alpha_t = \alpha_t(T_s, T_g, X, P_e) = \sum_{k=1}^{M}(f(T_s/\nu_{l,k}) - f(T_s/\nu_{u,k})) \tag{13}$$

The source temperature is set equal to the local gas temperature ($T_s = T_g$) when local properties are calculated. The upper and lower limits in Eq. 13 are calculated from Eq. 14 in case of a symmetric band where the center $\nu_{c,k}$ is specified.

$$\nu_{u,k} = \nu_{c,k} + \Delta\nu_k/2 \quad \text{and} \quad \nu_{l,k} = \nu_{c,k} - \Delta\nu_k/2 \tag{14}$$

All bands considered by the EWBM are symmetric except the 4.3 μm band of CO_2 that has an upper limit. For this asymmetric band, the remaining band limit is fixed by Eq. 15.

$$\nu_{u,k} - \nu_{l,k} = \Delta\nu_k \tag{15}$$

In Eqs. 14 and 15 $\Delta\nu_k = \nu_u - \nu_l = A_k$, that is the upper and lower limits of the "effective" bandwidth A_k are used rather than the true band limits. In the event two or more bands that overlap the minimum and maximum limits of the overlapping bands are used in Eq. 13, whereas the intermediate limits are disregarded. The f function in Eq. 13 represents a fraction of the black body emissive power. Analytical expressions for the calculation of the f function can be found in standard radiation textbooks.[23] The Wiebelt polynomials[23] are used in this work. Finally, the Beer's law is applied to calculate the total absorption coefficient via Eq. 16.

$$\kappa = \frac{1}{L}\ln\left(\frac{1}{1-\alpha_t}\right) \tag{16}$$

The BA method has been implemented in an individual programming code and the total absorption coefficient is

tabulated over the temperature range 1100–1900 K that is encountered in the industrial steam cracking furnace under consideration. A fixed flue gas composition is used in all simulations. This is justified by the fact that in furnaces with side-wall radiation burners, combustion is localized in the burner cups and hot flue gases consisting of combustion products only are released in the furnace box. In practice, the flue gas composition in the furnace remains unaltered. Complete combustion of the gaseous fuel in the burner cups is assumed. Furthermore, a pressure of 1 atm has been used in all simulations since the pressure drop in such a furnace does not exceed 50 Pa.[24] This minor pressure difference has a negligible impact on the calculated absorption coefficient. The above assumptions are taken advantage of and the total absorption coefficient is expressed by means of a temperature polynomial, which is very handy in CFD simulations. Nine absorption bands (five bands for CO_2 and four bands for H_2O) were initially considered for the calculation of the absorption coefficient. These bands are referred to as[23]:

$$CO_2: 15\ \mu m, 10.4\ \mu m, 9.4\ \mu m\ 4.3\ \mu\text{m}, 2.7\ \mu\text{m}$$

$$H_2O: 6.3\ \mu m, 1.87\ \mu\text{m}, 1.38\ \mu\text{m}, 2.7\ \mu\text{m}$$

It is found that a set of five bands, two of which overlap, yield a satisfactory approximation of the absorption coefficient for the conditions met in steam cracking furnaces over a wide range of mean beam lengths. These bands are:

$$CO_2: 15\ \mu\text{m}, 4.3\ \mu\text{m}, 2.7\ \mu\text{m}$$

$$H_2O: 6.3\ \mu\text{m}, 2.7\ \mu\text{m}$$

These bands are taken into account in the final implementation of the EWBM and the temperature polynomial (Eq. 17) that is calculated with the BA method is the final working equation for the gray gas model used in the further CFD calculations of the steam cracking furnace.

$$\kappa = 3.402 - 0.0024T + 5 \times 10^{-7}T^2 \tag{17}$$

The mean beam length L, which is required for the calculation of the absorption coefficient, is determined based on an approximated average cell volume in the calculation domain. $L = 6.8$ cm is used in this work. This value is actually somewhat higher than an approximated mesh spacing value calculated assuming a uniform square mesh as AMSV $= \sqrt[3]{\text{furnace volume}/\text{number of cells}}$. Another alternative is to use the mean beam length for the whole enclosure,[25] which is the furnace. The first approach has the disadvantage that the final outcome is somewhat dependent on the grid resolution, but it is consistent with the EWBM variant, which is applied here and has been developed for isothermal gas radiation. The latter condition is fulfilled in a cell volume or possibly in small cell clusters in given regions of the furnace domain, but cannot be assumed for the entire furnace domain. As a final remark, it is noted that neither of the approaches above is supported by sound physical reasoning, which actually renders the choice of the mean beam length value in the literature to be more or less arbitrary.

Table 1. Division of the Wavelength Spectrum into Four Gas Absorption Bands and Five "Clear" Windows

Band	Lower Limit, μm	Upper Limit, μm	Absorption Coefficient, m^{-1}
1	0	2.50	0
2	2.50	2.76	$9.4388 - 0.0035T + 8\ \text{E}\ -7T^2$
3	2.76	4.15	0
4	4.15	4.49	$12.763 + 0.0025T - 1\ \text{E}\ -6T^2$
5	4.49	5.02	0
6	5.02	8.32	$4.9413 - 0.0035T + 8\ \text{E}\ -7T^2$
7	8.32	11.80	0
8	11.80	20.66	$4.8798 - 0.0034\text{T} + 8\ \text{E}\ -7T^2$
9	20.66	45	0

Nongray gas modeling

Distinct absorption coefficients are derived for the four distinct absorption bands (15, 6.3, 4.3, 2.7 μm) that have been considered for the gray modeling approach as well. For the overlapping 2.7 μm band, the BA method is used to calculate a single absorption coefficient. In short, the band transmittance (Eq. 9) and the band width (Eq. 10) are calculated first over the range 1100–1900 K using the four region expression. Next, an average width for each band is computed and remains fixed for the recalculation of the band transmittances over the range 1100–1900 K using Eq. 12. It is noted here that the computed bandwidths do not change considerably with temperature and thus a simple arithmetic average bandwidth is considered representative for each band. In this approach, an arbitrary upper limit for the band transmittance, as explained before is not imposed. The fixed bandwidth is also used for the computation of fixed band limits over which the radiative transfer equation (RTE) is solved. Eventually, the Beer's law is used to calculate the band absorption coefficients. As in the gray modeling approach, the band coefficients are expressed in terms of temperature polynomials taking advantage of the nearly uniform concentration and pressure fields in the furnace. For the spectral "clear" windows, outside the limits of the absorbing bands, the absorption coefficient is set equal to zero. To make sure that the entire wavelength spectrum is covered by the bands, we choose $\lambda_{\min} = 0$ and $\lambda_{\max}T_{\min} = 50{,}000$.[26] Here $\lambda_{\min}$ and $\lambda_{\max}$ are the minimum and the maximum wavelength bounds of the wavelength spectrum, and $T_{\min}$ is the minimum expected temperature in the domain, which is taken equal to 1100 K in this work. The computed band limits and band absorption coefficients that are used in the context of nongray modeling are quoted in Table 1. It is also noted here that the maximum number of SBs, including clear windows, that can be implemented in FLUENT is 10.

Solution Method for the Radiative Transfer Equation

The discrete ordinates—finite volume method

To simulate the thermal radiation exchange, both in gray and nongray calculations, a conservative variant of the discrete ordinates (DO) radiation model, called the finite-volume (FV) scheme, implemented in the FLUENT software package, has been used. This is the only RTE solver in FLUENT that can be used to model nongray radiation. The finite vol-

ume method was originally introduced by Raithby and Chui[27] and is slightly modified and described in detail by Baek et al.[28] and Raithby.[29] The DO model considers the RTE in the direction $\vec{s}$ as a field equation[26]:

$$\nabla \cdot (I(\vec{r},\vec{s})\vec{s}) + (\kappa + \sigma_s) I(\vec{r},\vec{s}) = \kappa n^2 \frac{\sigma T^4}{\pi} + \frac{\sigma_s}{4\pi} \int_0^{4\pi} I(\vec{r},\vec{s}\,')\Phi(\vec{s}\cdot\vec{s}\,')d\Omega' \quad (18)$$

As is usually done, the time derivative on the LHS is neglected. When modeling nongray gas radiation, Eq. 18 is solved band wise, for the spectral intensity $I_\lambda(\vec{r},\vec{s})$, in the following form:

$$\nabla \cdot (I_\lambda(\vec{r},\vec{s})\vec{s}) + (\kappa_\lambda + \sigma_s) I_\lambda(\vec{r},\vec{s}) = \kappa_\lambda n^2 I_{b\lambda} + \frac{\sigma_s}{4\pi} \int_0^{4\pi} I_\lambda(\vec{r},\vec{s}\,')\Phi(\vec{s}\cdot\vec{s}\,')d\Omega' \quad (19)$$

Here κ_λ is the spectral absorption coefficient, and $I_{b\lambda}$ is the black body intensity given by the Planck function. The scattering coefficient σ_s, the scattering phase function Φ, and the refractive index n are assumed independent of the wavelength λ. The nongray implementation divides the radiation spectrum into N wavelength intervals. The RTE is integrated over each wavelength interval $\Delta\lambda$, resulting in transport equations for the quantity $I_\lambda \Delta\lambda$. The behavior in each absorbing band is assumed to be gray. The black body emission over the wavelength interval per unit solid angle is:

$$I_{b,\Delta\lambda} = (f(n\lambda_u T) - f(n\lambda_l T)) n^2 \frac{\sigma T^4}{\pi} \quad (20)$$

where λ_u and λ_l are the upper and the lower wavelength boundaries respectively of the considered wavelength interval, and $f(n\lambda T)$ is the fractional black body function. Finally, the total intensity in each direction $\vec{s}$ and position $\vec{r}$ is computed using Eq. 21.

$$I(\vec{r},\vec{s}\,) = \sum_N I_\lambda(\vec{r},\vec{s}\,)\Delta\lambda \quad (21)$$

where the summation is performed over all the wavelength bands.

Radiation boundary conditions

In case of gray gas radiation, modeling the radiative flux leaving a solid surface is:

$$q_{\text{out}} = (1 - \varepsilon_w) q_{\text{in}} + n^2 \varepsilon_w \sigma T_w^4 \quad (22)$$

where ε_w is the gray wall emissivity and q_{in} is the incident radiative heat flux at the surface that is calculated as:

$$q_{\text{in}} = \int_{\vec{s}\cdot\vec{n}>0} I_{\text{in}} \vec{s}\cdot\vec{n} d\Omega \quad (23)$$

The boundary conditions in case of nongray/DO modeling are applied on a band basis. The treatment of the boundary conditions within a gray band is the same as for gray radiation modeling. In case of nongray gas radiation modeling, the radiative flux leaving a surface within a wavelength band $\Delta\lambda$ is:

$$q_{\text{out},\Delta\lambda} = (1 - \varepsilon_{w,\Delta\lambda}) q_{\text{in},\Delta\lambda} + \varepsilon_{w,\Delta\lambda}(f(n\lambda_u T) - f(n\lambda_l T)) n^2 \sigma T_w^4 \quad (24)$$

where ε_w,$\Delta\lambda$ is the wall emissivity in the band and q_{in},$\Delta\lambda$ is the incident radiative heat flux at the surface within the band wavelength interval $\Delta\lambda$, which is calculated as:

$$q_{\text{in},\Delta\lambda} = \Delta\lambda \int_{\vec{s}\cdot\vec{n}>0} I_{\text{in},\lambda} \vec{s}\cdot\vec{n} d\Omega \quad (25)$$

CFD Modeling

A three-dimensional mathematical model is used to simulate the flow in the radiation section of the steam cracking furnace segment. The model consists of the partial differential equations describing the conservation of momentum, heat, and mass, in combination with a two-equation turbulence model. If the dependent variable is denoted by Φ, the general differential equation is:

$$\frac{\partial}{\partial t}(\rho\Phi) + \text{div}(\rho v\Phi - \Gamma_\Phi \text{grad}\Phi) = S_\Phi \quad (26)$$

where Γ_Φ is the diffusion coefficient and S_Φ is the source term. The turbulence kinetic energy and the dissipation of turbulence are calculated with the $k - \varepsilon$ model.[30] Standard wall functions are employed to model the near-wall region.[26,31] The boundary layers are resolved so that $y^* < 300$. The set of partial differential equations along with the boundary and inlet conditions is solved with the finite volume method using a segregated solver, the SIMPLE algorithm[32,33] for pressure–velocity coupling, and the second order upwind differencing discretization scheme for the convection operator. The above together with the DO-FV radiation model have been embodied in the general FLUENT CFD program.[26] The total and band absorption coefficients for the gray gas and nongray gas calculations respectively are calculated locally by means of temperature polynomials (Eq. 17 and Table 1, respectively) implemented in User Defined Functions (UDF). The latter are plugged into the FLUENT solver. Consequently, the RTE solver of FLUENT reads the total or band absorption coefficients from the respective UDF each time the RTE is solved. It is reminded that the RTE is solved separate from the flow equations. The temperature polynomials have been derived in a preprocessing step using the EWBM, which has been implemented in individual programming codes. In principle, the EWBM itself can be implemented in a UDF. In this work, this is not necessary because the local absorption coefficient variation is only because of the local temperature variation. As explained before, concentration and pressure profiles are nearly uniform in the furnace. Opaque, gray-diffuse furnace wall and tube skin surfaces are assumed in both gray gas and nongray gas calculations. The index of refraction is set to 1 and scattering is neglected. Finally, four N_θ and four N_ϕ divisions are found

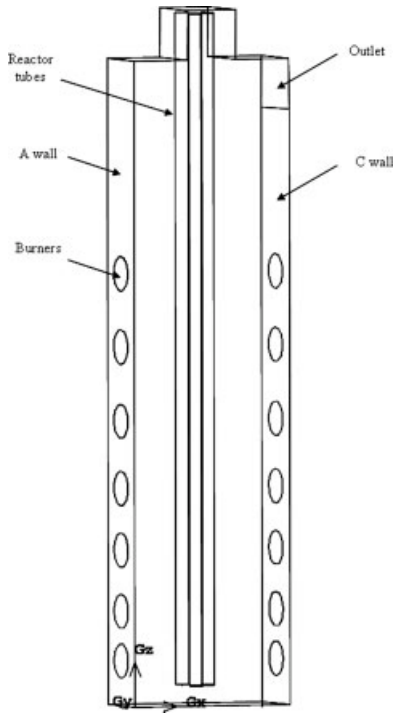

Figure 1. Simulated naphtha cracking furnace segment.

to be adequate for the problem studied. The angles θ and ϕ are the polar and azimuthal angles, respectively, and are measured with respect to the global Cartesian system. In three-dimensional calculations, a total of $8N_\theta N_\phi$ directions are solved. In case of the nongray model, a total of $8N_\theta N_\phi$ equations are solved for each band. Further angular discretization refinement shows no influence on the calculated results. Finally, all calculations are considered converged when the scaled residuals reduce to 10^{-3} for all equations except the energy and radiation intensity equations, for which the criterion is 10^{-6}.[26]

Furnace Geometry and Operating Conditions

A representative segment of an industrial naphtha cracking furnace with side-wall radiation burners is simulated. A schematic representation of this segment is given in Figure 1 and

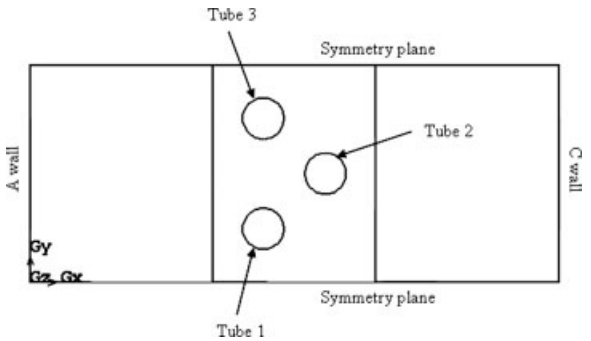

Figure 2. Top view of the simulated furnace segment.

Table 2. Simulation Conditions

Furnace segment	
Height, m (z)	7.32
Length, m (y)	0.7
Width, m (x)	1.7
Thickness of refractory, m	0.23
Thickness of insulation, m	0.05
Thickness of casing, m	0.005
Number of burners	14
Reactor	
Number of reactor tubes	3
External tube diameter,m	0.1319
Internal tube diameter, m	0.1143
Firing conditions	
Flue gas flow rate, kg/s	1.23242
Flue gas composition, wt %	
CO_2	0.1220
H_2O	0.1180
O_2	0.0366
N_2	0.7234
Flue gas inlet temperature, K	1871.84
Material properties	
Emissivity of furnace wall	0.6
Emissivity of tube skin	0.85
Thermal conductivity of refractory wall, W/m/K	0.394
Thermal conductivity of insulation, W/m/K	0.19
Thermal conductivity of casing, W/m/K	56
Thermal conductivity of tube skin, W/m/K	26.05

the top view of the segment is given in Figure 2. By considering two sides as symmetry planes, the furnace segment represents an infinitely long furnace. The furnace segment is

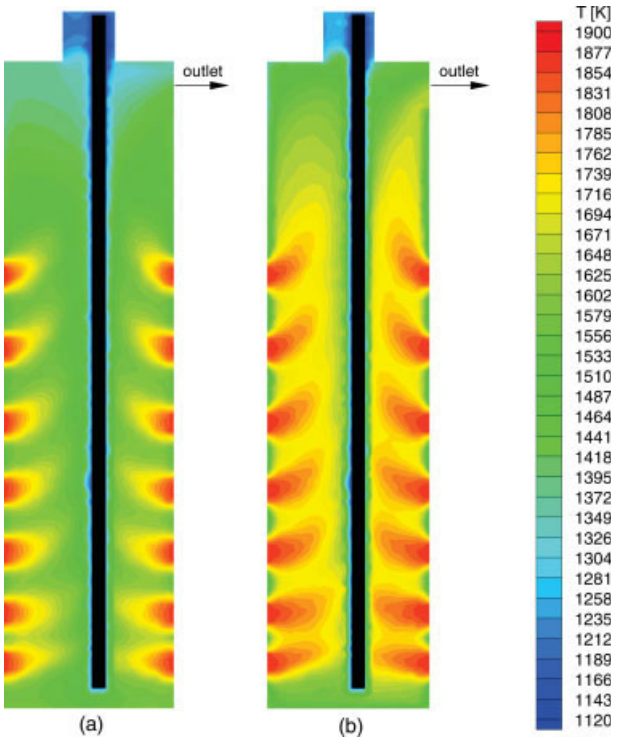

Figure 3. Temperature contour plots in a vertical cross section in the middle of the furnace at y = 0.35 m.

(a) Gray gas radiation model. (b) Nongray gas radiation model. Operating conditions: Table 2.

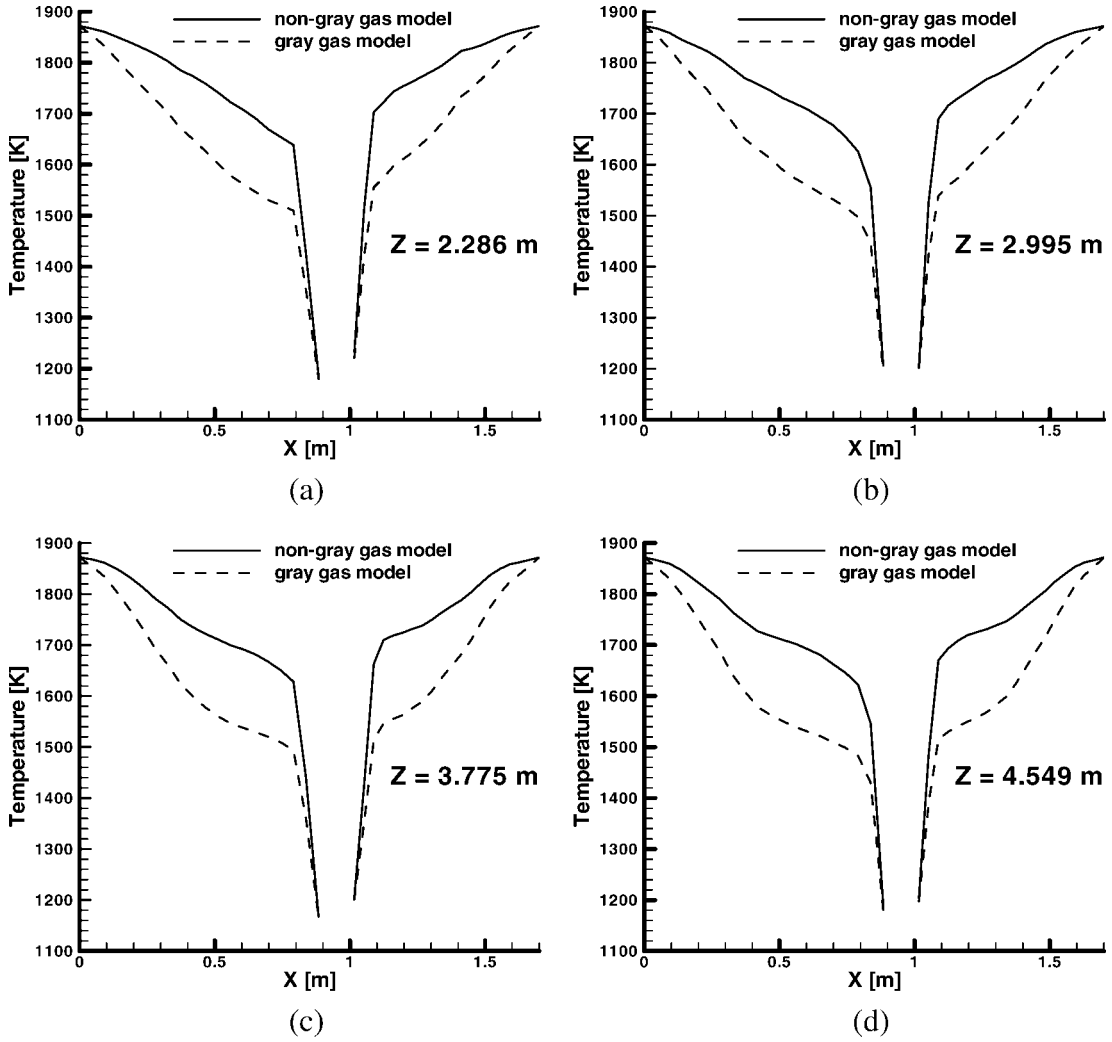

Figure 4. Flue gas temperature profiles along the width of the furnace at different heights.

The heights (z) in (a), (b), (c) and (d) correspond to the heights of the 4th, 5th, 6th and 7th burner respectively. $y = 0.35$ m. Operating conditions: Table 2.

heated with 14 radiation burners, positioned in one row of burners in the front wall (A wall) and one row of burners in the rear wall (C wall) of the furnace. The furnace outlet is located at the top of the C wall and runs across its entire length. Because of the high degree of turbulent mixing between fuel and oxidizer in the burner cups, complete combustion of the fuel gas in the cups can be assumed. This entails that only hot combustion products (hot flue gas) enter the radiation section of the furnace. The product species concentrations remain invariant in the simulated domain. Around 77,178 tetrahedral cells are used to discretize the physical domain between the furnace walls, the symmetry plane, and the reactor tubes. In this work, no coupled furnace/reactor simulation[3,4] is performed, as only a segment of the furnace is simulated. Therefore, a fixed internal tube skin temperature is applied and is considered to be a part of the boundary conditions of the simulations. The basic simulation conditions concerning the furnace segment dimensions and the operating conditions are given in Table 2.

Results and Discussion

As mentioned in the introduction, the goal of this work is to quantify the effect of the gray gas simplification on important furnace design parameters like the temperature distribution in the fire box, the flue gas flow pattern, and the heat fluxes from the flue gas to the reactor tubes. These parameters determine the conversion of naphtha in the reactor coils and have an important influence on detrimental side effects as the coke formation on the internal tube surface. First, in Figure 3, the temperature contour plots for the gray and nongray gas calculations in a vertical plane in the middle of the furnace at $y = 0.35$ m (see Figures 1 and 2) through the burners and the middle tube are shown. It can readily be observed that the flue gas temperatures that are calculated with the nongray gas model are higher than those that are calculated with the gray gas model.

A more quantitative view of the temperature distribution in the firebox is given in Figure 4, where horizontal temperature profiles along the x-direction at $y = 0.35$ m and at sev-

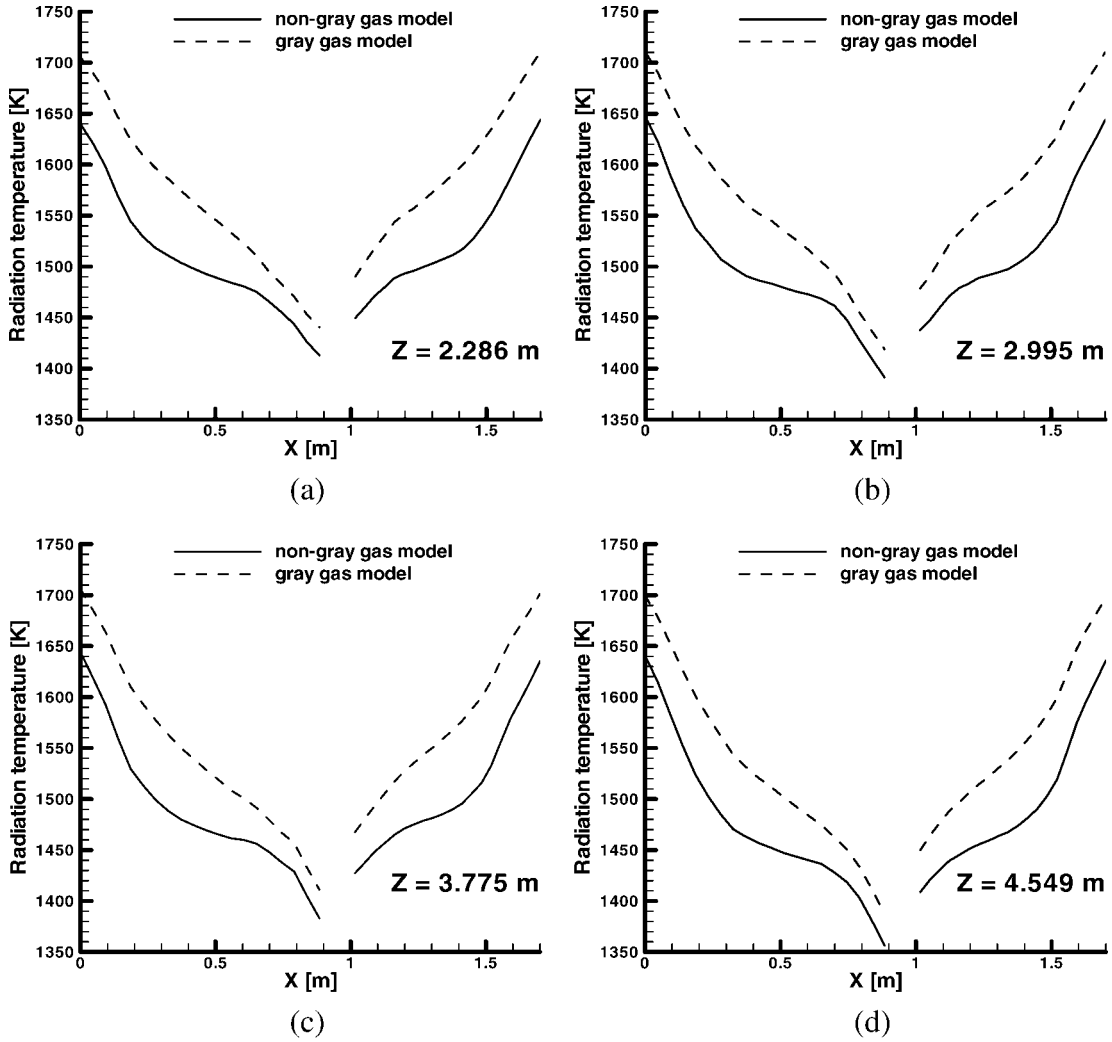

Figure 5. Radiation temperature profiles along the width of the furnace at different heights.

The heights (z) in (a), (b), (c) and (d) correspond to the heights of the 4th, 5th, 6th, and 7th burner respectively. $y = 0.35$ m. Operating conditions: Table 2.

eral heights are presented. The temperature lines in Figures 4a–d connect the centers of the 4th, 5th, 6th, and 7th burner (Figure 1) of the front (A) wall with the centers of corresponding burners on the rear (C) wall. Both modeling approaches predict decreasing flue gas temperatures when leaving the burners' area and approaching the center (with respect to the x-direction) of the furnace. In the center of the furnace where the reactor tubes are situated a steep temperature drop, the so-called "heat sink" is predicted in both cases. However, the use of a nongray gas radiation model results in a completely different flue gas temperature profile between the front wall and the rear wall. This difference in the shape of the flue gas temperature profile is observed at several heights of the furnace box. More specifically, it is observed in Figures 4a–d that the temperature lines diverge from one another while moving away from the wall and converge again in the "heat sink" zone close to the tubes. Outside the "heat-sink" zone a convex type of flue gas temperature profile is predicted with the nongray gas model, whereas a concave type of flue gas temperature profile is predicted with the gray gas model. These trends are in agreement with those reported in a previous work of Heynderickx and Nozawa[18] for a complete furnace/reactor simulation with radiation burners. This is remarkable considering the fact that in that work a completely different overall modeling approach was followed. A simplified plug flow assumption for the flue gas flow in the furnace was considered.[18] However, an advanced radiation model based on the zone method of Hottel and Sarofim[34] and a Monte Carlo simulation for the calculation of the radiative heat exchange in the furnace was used. Continuing the discussion of Figure 4, it is also remarked that higher temperature values are calculated with the nongray gas model along the entire x-axis. The calculated temperature differences, which exceed 150 K in some areas, are most pronounced in the zones between $x = 0.4$ m and $x = 0.8$ m, approximately, on the left of the tube and between $x = 1.05$ m and $x = 1.4$ m, approximately, on the right of the central tube (flue gas outlet side).

Higher flue gas temperatures in the furnace domain when using the nongray gas model imply that more radiation energy

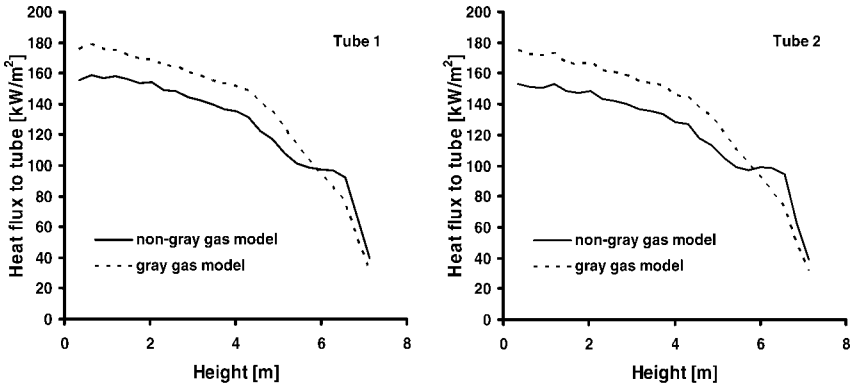

Figure 6. Tube heat flux profiles along tube length (*z*-direction).

Solid lines: nongray gas model. Dashed lines: gray gas model. Operating conditions: Table 2.

is absorbed by the flue gas because of the high absorption coefficients in the strongly absorbing bands of 2.7 and 4.3 μm (calculated by the temperature polynomials in Table 1). This argument is supported by Figures 5a–d, which correspond to Figures 4a–d. In Figures 5a–d, horizontal radiation temperature profiles at $y = 0.35$ m and at the same heights as the flue gas temperature profiles of Figures 4a–d are presented. Radiation temperature of a body is the temperature that a blackbody of similar dimensions would have that radiated the same intensity at the same frequency and is defined by:

$$\theta_R = \left(\frac{G}{4\sigma}\right)^{1/4} \tag{27}$$

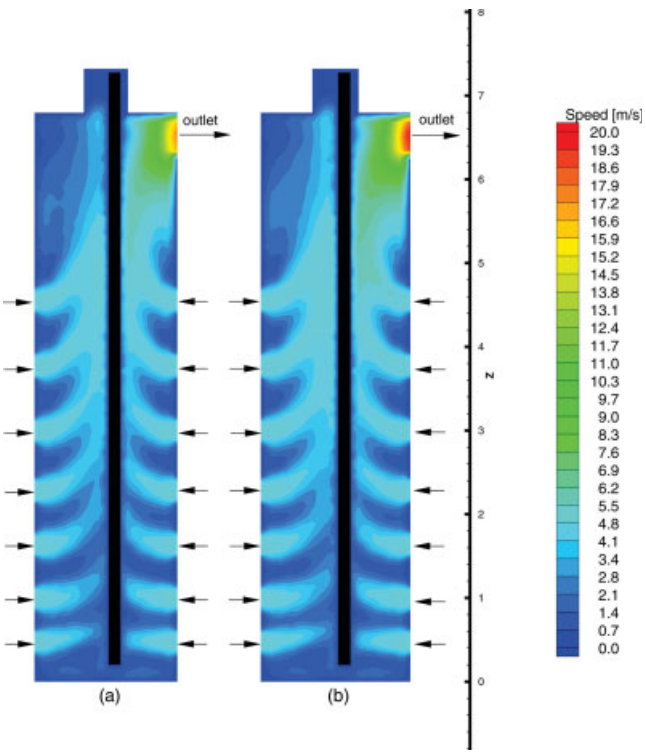

Figure 7. Flue gas speed (velocity norm) contour plots in a vertical cross section in the middle of the furnace at $y = 0.35$ m.

(a) Gray gas radiation model. (b) nongray gas radiation model. The arrows on the two sides of the plots indicate the burner openings. Operating conditions: Table 2.

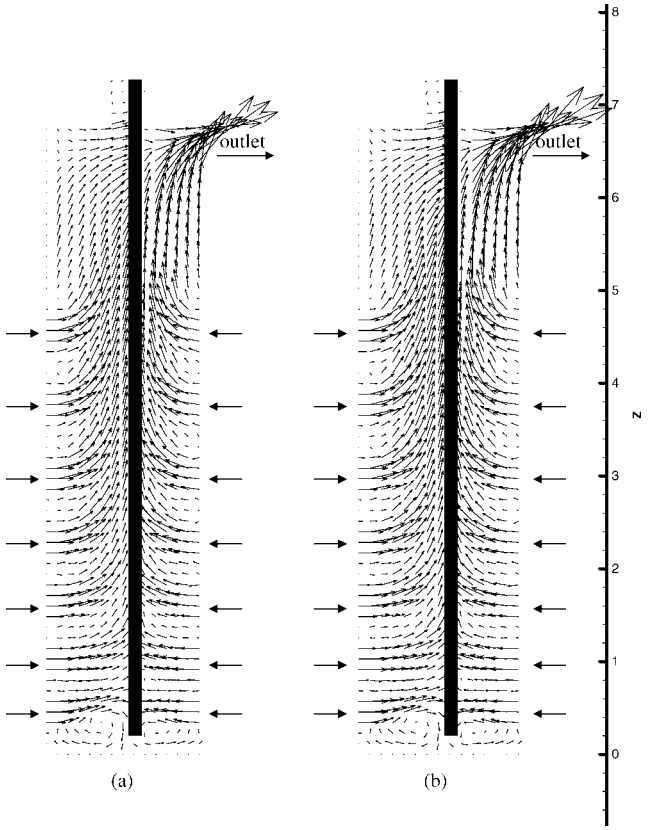

Figure 8. Flue gas velocity vector plots in a vertical cross section in the middle of the furnace at $y = 0.35$ m.

(a) Gray gas radiation model. (b) nongray gas radiation model. The arrows on the two sides of the plots indicate the burner openings. Operating conditions: Table 2.

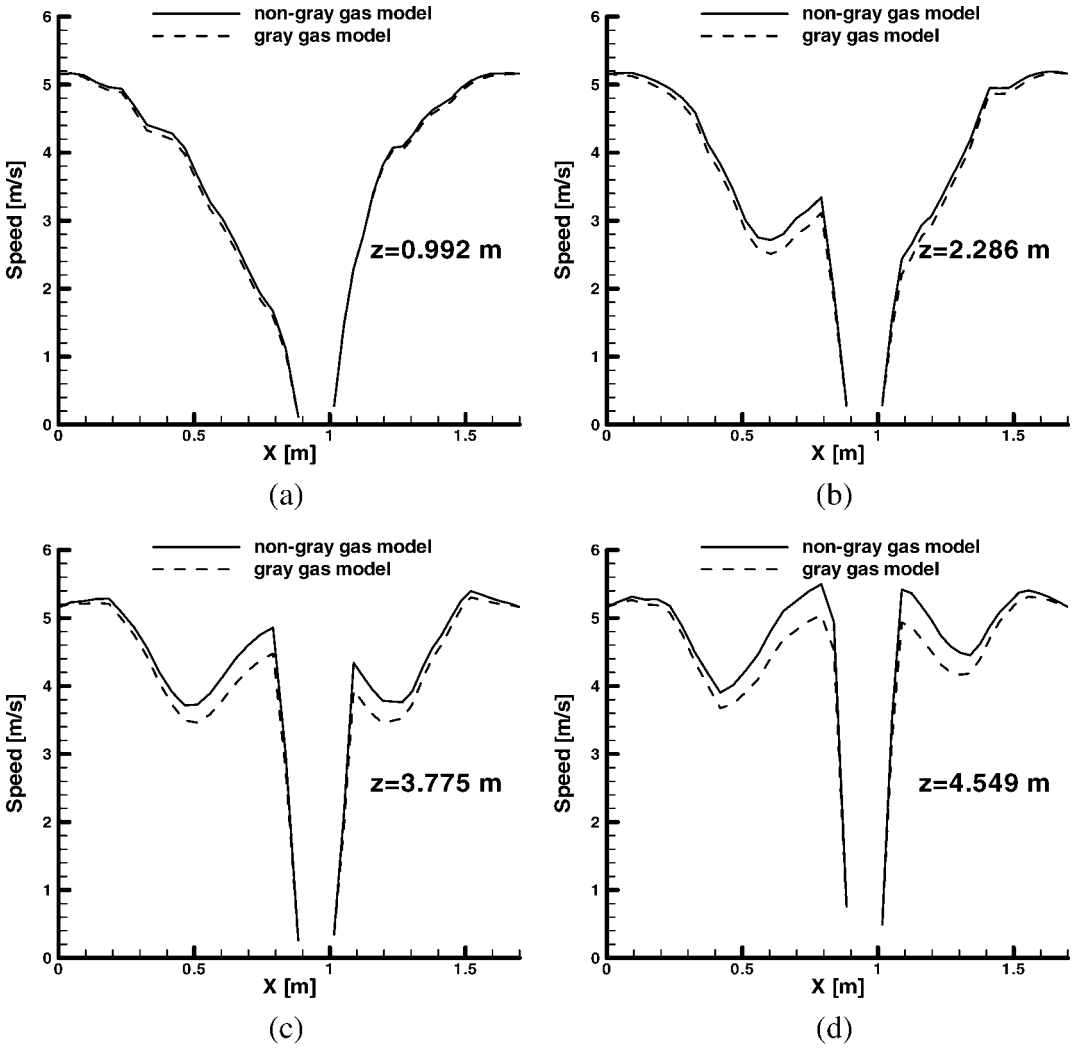

Figure 9. Flue gas speed (velocity norm) profiles along the width of the furnace at different heights.

The heights (z) in (a), (b), (c) and (d) correspond to the heights of the 2nd, 4th, 6th and 7th burner respectively. $y = 0.35$ m. Operating conditions: Table 2.

where G is the incident radiation namely, the total radiation energy that arrives at a location per unit time per unit area and is defined by:

$$G = \int_{\Omega=4\pi} I d\Omega \tag{28}$$

Lower radiation temperatures when using the nongray gas model all along the x-axis (Figure 5a–d) indicate lower values for the incident radiation, being the numerator in Eq. 27. The latter entails that more radiation energy, G, is absorbed by the gas resulting in higher temperatures in the furnace domain than those that are calculated with the gray gas model (Figures 3 and 4). On the contrary, when using the gray gas model less radiation energy is absorbed by the flue gas and more radiation is transferred to the reactor tubes. This is shown in Figure 6 where the profiles of heat flux to tube 1 and tube 2 (Figure 2) with the gray gas and nongray gas models are plotted. The line representing the heat flux profile with the nongray gas model is lower than that representing the heat flux profile with the gray gas model along the tube height with the exception of a short zone lying between 6 m height and the top of the tube. The descending heat flux profile trend versus tube height that is predicted with both models is because of the fact that the distance between successive burners increases with height and the fact that the highest burner is situated at 4.549 m height, whereas the total furnace height is 7.32 m. Overall, the predicted furnace thermal efficiency namely, the fraction of the energy input to the furnace that goes to the tubes, rises from 37.5% when using the nongray gas model to 42.6% when using the gray gas model. The difference of 5% in thermal efficiency that is predicted is large considering the scale and the importance of the industrial process and should be taken into account by the furnace designer. It should be mentioned here that the exact difference in thermal efficiency values can and will be somewhat different when a complete coupled furnace/reactor simulation is performed for the steam cracking process. However, the qualitative and quantitative assessment of the gray gas approximation for steam cracking furnace calculations can be carried out effectively in the context of furnace segment simulations.

This work is completed with a discussion on the flow patterns in the furnace as they are predicted when using the gray and nongray gas radiation model. The discussion is supported by Figures 7–9. Figure 7 shows the contour plots of flue gas speed (velocity norm) in a vertical plane in the middle of the furnace at $y = 0.35$ m. Figure 8 shows the velocity vector plots in the same vertical plane and finally Figure 9 shows horizontal profiles of flue gas speed at different heights in the same plane. Four major elements that characterize the flue gas flow in the furnace can be identified and they are qualitatively predicted by both radiation models (Figures 7 and 8). These elements are:

a. Two recirculation zones in between each one of the lowest burners on the left and right half side of the furnace and the furnace floor.
b. The gradual flow acceleration with furnace height in the center zone lying between $x = 0.4$ m and $x = 1.3$ m. The acceleration is more pronounced on the left hand side of the furnace and is more clearly shown in Figure 9.
c. The major shift of fluid flow from the left half of the furnace to the right one, where the outlet is located, from the level of the top burner and higher.
d. The peak flue gas speed region that occurs close to the furnace outlet because of the sudden contraction of the flow domain. In fact, what is called furnace outlet in this work is a narrow cross zone in between the radiation and the convection section of the furnace.

Although the above flow characteristics are predicted by both models, quantitative differences in the predicted flue gas speed profiles do exist and are shown in Figure 9. It is shown that the difference in flue gas speed increases with increasing height and becomes more pronounced as the tube zone is approached. At the height level of the second burner at $z = 0.992$ m, the predicted difference in the flue gas speed is negligible, whereas 3.5 m higher approximately, at the height of the top burner, the difference has risen to 0.5 m/s. This difference in the flue gas speed is because of the fact that the higher flue gas temperatures that are predicted with the nongray gas model result in bigger flue gas expansion. The maximum flue gas speed that is predicted with the gray gas model in the flow domain is 18.52 m/s, whereas the maximum flue gas speed that is predicted with the nongray gas model is 20.77 m/s. Both peak speeds take place at the furnace outlet.

Conclusions

A constant composition gray gas and a constant composition nongray gas radiation model have been developed and applied in the context of CFD simulations of an industrial scale steam cracking furnace segment. Both models are based on the exponential wide band model of Edwards. The effect of the gray gas approximation, which is commonly used for simulations of industrial applications, on predicted fields like flue gas flow, temperature, and heat flux to the reactor tubes has been quantified. These variables are important parameters for the optimal design and operation of furnaces. When the gray gas simplification is used, less energy absorption by the flue gas in the furnace box and more energy transfer to the process gas in the reactor tubes are calculated. Thus, the calculated thermal efficiency increases from 37.5% when using the nongray gas model to 42.6% when using the gray gas model. The 5% difference in the predicted thermal efficiency is large considering the scale and the importance of the industrial process. It should be taken into account by the furnace designers that the gray gas simplification leads to deviations in the simulation results. It has also been shown that although both models reproduce the basic characteristics of the flow pattern in the furnace, noticeable quantitative differences in the flue gas speed are predicted in some regions of the furnace domain.

Notation

A^* = dimensionless band absorption
A = band absorption or "effective bandwidth", m^{-1}
b = self-broadening to foreign-gas broadening ratio
d = spectral line spacing, m^{-1}
$f(T/v)$ = fraction of the black body emissive power
G = incident radiation, $J/m^2/s$
I = radiation intensity, $J/m^2/s$
k = production rate of turbulent kinetic energy, m^2/s^2
L = mean beam length, m
N = number of bands
N_θ = number of polar angles
N_ϕ = number of azimuthal angles
n = empirical factor
refractive index
$\vec{n}$ = normal pointing out of the domain
P_e^* = equivalent broadening pressure parameter
P = pressure, Pa
P_a = absorber partial pressure, Pa
P_0 = reference partial pressure, 101,325 Pa
q = heat flux, W/m^2
$\vec{r}$ = position vector
$\vec{s}$ = direction vector
$\vec{s}'$ = scattering direction vector
S = source term
line intensity, m/kg
S/d = line intensity to line spacing ratio, m^2/kg
T = temperature, K
t = time, s
x^* = absorber mole fraction, $x = P_a/P$
X^* = density beam length, kg/m^2
y^* = dimensionless group in wall functions

Greek letters

α = integrated band intensity, m/kg
α_t = total absorptance
β = mean line width to spacing parameter
γ = line half width, m^{-1}
Γ = diffusion coefficient
Δ = difference operator
ε = emissivity
dissipation rate of turbulent kinetic energy m^2/s^3
η^* = the quantity βP_e
κ = absorption coefficient, m^{-1}
λ = wavelength, m
v = wavenumber, m^{-1}
ρ = gas density, kg/m^3
σ = Stefan-Boltzmann constant, $\sigma = 5.67 \times 10^{-8}$, $J\ s^{-1}\ m^{-2}\ K^{-4}$
σ_s = scattering coefficient, m^{-1}
τ_H^* = maximum optical depth at the band head
τ = transmittance
$\vec{v}$ = overall velocity vector, m/s
Φ = phase function
ϕ = dependent variable

ω = exponential decay width, m^{-1}
Ω' = solid angle, sr
Ω = hemispherical solid angle, sr

The variables marked with an asterisk (except the variable y) are composition dependent variables in the EWBM.

Subscripts

0 = reference value, origin
h = black body
c = center
g = gas
k = gas band
l = lower
min = minimum
max = maximum
s = source
path length
t = total
u = upper
w = wall
λ = spectral

Abbreviations

AMSV = approximated mesh spacing value
BA = block approximation
BCP = block calculation procedure
BEA = band energy approximation
CFD = computational fluid dynamics
DO = discrete ordinates
EWBM = exponential wide band model
FV = finite volume
HITRAN = hIgh resolution TRANSmission molecular absorption database
NB = narrow band
RTE = radiative transfer equation
SB = spectral band
SIMPLE = semi implicit method for pressure linked equations
SLBL = spectral line by line
SLW = spectral line-based weighted sum of gray gases
UDF = user defined function
WB = wide band
WSGG = weighted sum of gray gases

Literature Cited

1. Van Geem KM, Heynderickx GJ, Marin GB. Effect of radial temperature profiles on yields in steam cracking. *AIChE J*. 2004;50:173–183.
2. Stefanidis GD, Merci B, Heynderickx GJ, Marin GB. CFD simulations of steam cracking furnaces using detailed combustion mechanisms. *Comput Chem Eng*. 2006;30:635–649.
3. Heynderickx GJ, Oprins AJM, Dick E, Marin GB. Three-dimensional flow patterns in cracking furnaces with long flame burners. *AIChE J*. 2001;47:388–400.
4. Oprins AJM, Heynderickx GJ, Marin GB. Three-dimensional asymmetric flow and temperature fields in cracking furnaces. *Ind Eng Chem Res*. 2001;40:5087–5094.
5. Hartmann JM, Di Leon RL, Taine J. Line-by-line and narrow-band statistical model calculations for H_2O. *J Quant Spectrosc Radiat Transfer*. 1984;30:119–127.
6. Rothman LS, Gamache RR, Tipping RH, Rinsland CP, Smith MAH, Benner DC, Devi VM, Flaud JM, Camy-Peyret C, Perrin A, Goldman A, Massie ST, Brown LR. The HITRAN molecular data base: editions of 1991 and 1992. *J Quant Spectrosc Radiat Transfer*. 1992;48:469–507.
7. Elsasser WM. Heat Transfer by Infrared Radiation in the Atmosphere. Cambridge MA:Harvard University Press, 1943.
8. Modest MF. Radiative Heat Transfer. New York: Academic Press, 2003.
9. Goody RM. *Atmospheric Radiation*. London: Oxford University Press, 1964.
10. Malkmus W. Random Lorenz band model with exponential-tailed S^{-1} line-intensity distribution function. *J Opt Soc Am*. 1967;57:323–329.
11. Edwards DK. Molecular gas band radiation. *Adv Heat Transfer*. 1976;12:115–193.
12. Domoto GA. Frequency integration for radiative transfer problems involving homogeneous non-grey gases: The inverse transformation function. *J Quant Spectrosc Radiat Transfer*. 1974;14:935–942.
13. Goody R, West R, Chen L, Crisp D. The correlated-k method for radiation calculations in non-homogeneous atmospheres. *J Quant Spectrosc Radiat Transfer*. 1989;42:539–550.
14. Soufiani A, Taine J. High temperature gas radiative property parameters of statistical narrow-band model for H_2O, CO_2 and CO, and correlated-K model for H_2O and CO_2. *Int J Heat Mass Transfer*. 1997;40:987–991.
15. Smith TF, Shen ZF, Friedman JN. Evaluation of coefficients for the weighted sum of grey gases model. *J Heat Transfer*. 1982;104:602–608.
16. Denison MK, Webb BW. A spectral line-based weighted-sum-of-grey-gases model for arbitrary RTE solvers. *J Heat Transfer*. 1993;115:1004–1012.
17. Coelho PJ. Numerical simulation of radiative heat transfer from non-gray gases in three-dimensional enclosures. *J Quant Spectrosc Radiat Transfer*. 2002;74:307–328.
18. Heynderickx GJ, Nozawa M. Banded gas and nongrey surface radiation models for high-emissivity coatings. *AIChE J*. 2005;51:2721–2736.
19. Edwards DK, Balakrishnan A. Thermal radiation by combustion gases. *Int J Heat Mass Transfer*. 1973;16:25–40.
20. Ströhle J, Coelho PJ. On the application of the exponential wide band model to the calculation of radiative heat transfer in one- and two-dimensional enclosures. *Int J Heat Mass Transfer*. 2002;45:2129–2139.
21. Lallemant N, Weber R. A computationally efficient procedure for calculating gas radiative properties using the exponential wide band model. *Int J Heat Mass Transfer*. 1996;39:3273–3286.
22. Nilson TK, Sundén B. Modeling of thermal radiation properties of gases: The exponential wide band model (EWBM). *Int J Heat Technol*. 2003;21:1–10.
23. Siegel R, Howell JR. *Thermal radiation heat transfer*. New York: McGraw-Hill, 1972.
24. Oprins AJM, Heynderickx GJ. Calculation of three-dimensional flow and pressure fields in cracking furnaces. *Chem Eng Sci*. 2003;58:4883–4893.
25. Liu F, Becker HA, Bindar Y. A comparative study of radiative heat transfer modeling in gas-fire furnaces using simple grey gas and weighted-sum-of-grey-gases models. *Int J Heat Mass Transfer*. 1998;41:3357–3371.
26. Fluent Inc. *Fluent 6.2 User's Guide*. Lebanon, NH: Fluent Inc., January 2005.
27. Raithby GD, Chui EH. A finite-volume method for predicting a radiant heat transfer in enclosures with participating media. *J Heat Transfer*. 1990;112:415–423.
28. Baek SW, Kim MY, Kim JS. Nonorthogonal finite-volume solutions of radiative heat transfer in a three-dimensional enclosure. *Numer Heat Transfer B*. 1998;34:419–437.
29. Raithby GD. Discussion of the finite-volume for radiation, and its application using 3D unstructured meshes. *Numer Heat Transfer B*. 1999;35:389–405.
30. Markatos NC. The mathematical modelling of turbulent flows. *Appl Math Model*. 1986;10:190–220.
31. Launder BE, Spalding DB. The numerical computation of turbulent flows. *Comput Methods Appl Mech Eng*. 1974;3:269–289.
32. Markatos NC. Mathematical modelling of single- and two-phase flow problems in the process industries. *Revue De L'Institute Français Du Pétrole*. 1993;48:631–662.
33. Theologos KN, Markatos NC. Advanced modeling of fluid catalytic cracking riser-type reactors. *AIChE J*. 1993;39:1007–1017.
34. Hottel HC, Sarofim AF. *Radiative transfer*. New York: McGraw-Hill, 1967.

Manuscript received Nov. 9, 2006, and revision received Mar. 29, 2007.